Relative Position and Attitude Coupled Control for Autonomous Docking with a Tumbling Target

LU Wei, GENG Yunhai, CHEN Xueqin and ZHANG Fan

Research Centre of Satellite Technology,
Harbin Institute of Technology, Harbin, China
luwei.spacecraft@gmail.com, gengyh@hit.edu.cn, cxqhit@163.com, autoctrllab@gmail.com

Abstract

An integrated coupled control strategy for a servicing spacecraft autonomously approaching and docking with a freely tumbling target is studied. To implement capturing successfully, the docking port of the servicing spacecraft should be always pointing to the docking port of target during close rendezvous and docking, which involves proximity maneuvering of coupled position and attitude simultaneously. The integrated coupled control is accomplished through a robust sliding mode control for coupled relative position and attitude tracking. In order to design the integrated coupled control law, the integrated coupled dynamics of relative position and attitude is established through relative position vector and relative attitude quaternion. Then, based on the integrated coupled dynamics, an integrated coupled control law is designed through a robust sliding mode control technique which is constructed by two sliding surfaces. The convergence of sliding surfaces and tracking error are guaranteed in presence of unknown but bounded disturbances and model uncertainties. The robustness of the proposed control law to measurement noise is also analyzed. Finally, three numerical simulation scenarios are conducted and the results validate the effectiveness and robustness of the integrated coupled control law.

Keywords: *spacecraft; autonomous docking; integrated coupled control; sliding mode control; robustness*

1. Introduction

Autonomous servicing for a freely tumbling target in orbit has become an important research topic in recent years due to rapid increase of space activity. Among this area, autonomous approaching and docking is a key technology of autonomous on-orbit servicing. It's a challenging work to design the controller for coupled relative position and attitude dynamics, especially for the case of docking with a tumbling target. Typical missions which could be related with this include removing space debris, inspecting satellite, repairing failure satellite, replacing equipments of satellite, or refueling a powerless satellite and so on. Several such kinds of space programs to demonstrate the key technologies, such as NASA's DART [1], Air AFRL XSS-10 [2] and XSS-11 [3], DARPA's OE [4, 5], MIT's SPHERES [6] have already been performed.

In order to ensure successfully capturing the tumbling target, it's necessary to make the docking port of servicing spacecraft point to the docking port of target during close rendezvous and docking. This is the docking condition. The docking condition implies that the successfully capturing depends on the relative position and attitude

simultaneously. In fact, the relative position tracking command depends on not only the final relative position, but also the relative attitude. This kind of coupling, exited in relative position tracking command and attitude, is called pointing coupling. Furthermore, the relative position and attitude dynamics of the servicing spacecraft with respect to target is also coupled, which is induced by the orbit thrusters fixed in the body-fixed frame of the servicing spacecraft. This kind of coupling is called dynamics coupling. In this paper, an integrated coupled control scheme, which is a combination of coupled relative position and attitude tracking, is proposed to solve the problem of a servicing spacecraft autonomous approaching and docking with a tumbling target. And both of the pointing coupling and dynamics coupling are considered.

It's well known that the phase of approaching to a tumbling target involves large angular maneuvers. In this case, the relative position and attitude motion involves highly nonlinear kinematics and dynamics, and linear control method is unsuitable for precise control. So, the nonlinear control method is necessary to investigate and to design the coupled control law. And lots of nonlinear control techniques have already been presented in literature to design controllers for nonlinear system. Such as, sliding mode control[7,8,9], H_∞ inverse optimal control [10], nonlinear robust control[11], nonlinear model predictive control [12], nonlinear model reference adaptive control [13], backstepping control [14] and so on.

Several research works related to rendezvous and docking are reviewed as follows. Terui [15] investigated the position and attitude tracking for the mission of capturing and removing large space debris, however, a normal sliding mode control was utilized. To the same mission, Stansbery and Cloutier [16] designed both position and attitude controller through the state-dependent Riccati equation (SDRE) technique which is a suboptimal optimal control for nonlinear system. And they all only considered the rigid body's motion coupling which is induced by the motion of spacecraft. The motion coupling exists in every spacecraft's motion, and it seldom affects the rigid body's motion. So, generally, it's unnecessary to consider the motion coupling when investigating the controller design. However, the pointing coupling and dynamics coupling, which can't be ignored and decides whether the capturing can be successful, was not considered in the previously mentioned literatures. Singla et al. [17] developed an output feedback structured model reference adaptive control law for spacecraft rendezvous and docking problem, and focus on analyzing the effect of bounded output errors on controller performance, the related coupling was not considered too. Excitedly, the breakthrough work was done by Subbarao and Welsh [18], they proposed a synchronization maneuvers scheme to solve the problem of relative position tracking and attitude reorientation for free-flying robotic spacecraft and serviceable objects in space. And the pointing coupling was considered in their research paper. Regret that the dynamics coupling was not included and the value of the control input was too large to implement in practice. Xin and Pan [19] proposed a nonlinear optimal control technique called $\theta - D$ to design a closed-form feedback control law for the control of translational, rotational and flexible vibrations simultaneously in one unified framework. However, the previously mentioned dynamics coupling was also not considered, and the simulation results in their paper show that the transient response of relative position, accompanying with large oscillation, was not stationary during approaching.

In this paper, the integrated coupled dynamics of relative position and attitude is established through relative position vector and relative attitude quaternion. Based on the integrated coupled dynamic model, a robust sliding mode control technique, which

is extension of Brown's method [20], is employed to design the integrated coupled control law. The robustness of the integrated coupled control law to bounded disturbances and model uncertainties are analyzed, and robustness to measurement noise is also investigated. And the problem of control constraint is effectively solved using Wie and Lu's method [21].

Rest of the paper is organized as follows. In Section 2, the problem description is given, including the relevant coordinate frames, governing equations of motion, and control objective. The integrated coupled dynamics of relative position and attitude is established in Section 3 and an integrated coupled control law, based on a robust sliding mode control method, for relative position and attitude is designed in Section 4. Simulation results and analysis are presented in Section 5. Conclusion is given in Section 6.

2. Problem Description

The problem to be studied is to control the relative position and attitude simultaneously to accomplish the docking condition. Although, the tumbling target is out of control, its state information including position, velocity, attitude and angular velocity can be obtained from target's sensors or servicing spacecraft's observation and estimation [22, 23, 24, 25, 26].

In order to describe the motion of servicing spacecraft with respect to target, the following coordinate systems are defined.

(1) The Earth-centered inertial coordinate system is denoted as $Ox_Iy_Iz_I$ and is fixed to the centre of the Earth. The Ox_I axis points toward the vernal equinox, the Oz_I axis extends through the North Pole, the Oy_I axis completes the triad.

(2) local-vertical-local-horizontal (LVLH) coordinate frame attached to the target is denoted as $O_Tx_Ly_Lz_L$. The O_Tx_L axis is directed along the radius vector of the target from the Earth's centre, the O_Tz_L axis is the direction of the orbital normal, and the O_Ty_L axis completes the triad.

(3) Body-fixed coordinate frames of servicing spacecraft and target are denoted as $O_Sx_{bs}y_{bs}z_{bs}$ and $O_Tx_{bt}y_{bt}z_{bt}$, respectively. Without loss of generality, it is assumed that x_{bs} axis of servicing spacecraft and $-x_{bt}$ axis of target are their respective outward normal direction of the docking ports. During the proximity operation, x_{bs} axis must always face the $-x_{bt}$ axis, or x_{bs} axis has the same direction with x_{bt} axis.

2.1. Relative Position Dynamics

The relative position dynamics is developed based on the relative position and velocity of the servicing spacecraft with respect to the LVLH frame fixed to target. Define $\boldsymbol{\rho} \in \mathbb{R}^3$ is the relative position vector from the target's center to the servicing spacecraft's center. $\boldsymbol{\rho}_L = [x, y, z]^{\mathrm{T}}$ is $\boldsymbol{\rho}$ expressed in the LVLH frame. The nonlinear equations of relative position dynamics in the absence of perturbation are described as[17]

$$\ddot{x} - 2\dot{\theta}\dot{y} - \ddot{\theta}y - \dot{\theta}^2 x = -\frac{\mu(R_T + x)}{\left[(R_T + x)^2 + y^2 + z^2\right]^{3/2}} + \frac{\mu}{R_T} + a_{cx} \tag{1}$$

$$\ddot{y} + 2\dot{\theta}\dot{x} + \ddot{\theta}x - \dot{\theta}^2 y = -\frac{\mu y}{\left[\left(R_T + x\right)^2 + y^2 + z^2\right]^{3/2}} + a_{cy} \tag{2}$$

$$\ddot{z} = -\frac{\mu z}{\left[\left(R_T + x\right)^2 + y^2 + z^2\right]^{3/2}} + a_{cz} \tag{3}$$

where μ is gravitational parameter, $\boldsymbol{a}_L = \left[a_{cx}, a_{cy}, a_{cz}\right]^{\mathrm{T}}$ is control acceleration of the servicing spacecraft expressed in the LVLH frame. R_T is the distance from the Earth centre to the target. Assuming θ is true anomaly of target orbit, the evolution of target orbit is governed by

$$\ddot{R}_T = R_T\dot{\theta} - \mu / R_T^{\,2} \tag{4}$$

$$\ddot{\theta} = -2\dot{R}_T\dot{\theta} / R_T \tag{5}$$

During approaching and capturing, the distance between the servicing spacecraft and target is very small, so $R_T \gg x, R_T \gg y, R_T \gg z$. After a few manipulations, and adding the external perturbations to the dynamic equations, the relative position dynamics of the servicing spacecraft with respect to the target expressed in LVLH frame can be described as

$$\ddot{\boldsymbol{\rho}}_L + \boldsymbol{A}_2\dot{\boldsymbol{\rho}}_L + \boldsymbol{A}_1\boldsymbol{\rho}_L = \boldsymbol{a}_L + \boldsymbol{f}_L \tag{6}$$

where $\boldsymbol{f}_L$ is the relative perturbation acceleration in the LVLH frame, and

$$\boldsymbol{A}_1 = \begin{bmatrix} -\dot{\theta}^2 - 2\mu / R_T^{\,3} & -\ddot{\theta} & 0 \\ \ddot{\theta} & -\dot{\theta}^2 + \mu / R_T^{\,3} & 0 \\ 0 & 0 & \mu / R_T^{\,3} \end{bmatrix} \tag{7}$$

$$\boldsymbol{A}_2 = \begin{bmatrix} 0 & -2\dot{\theta} & 0 \\ 2\dot{\theta} & 0 & 0 \\ 0 & 0 & 0 \end{bmatrix} \tag{8}$$

2.2. Relative Attitude Dynamics

The attitude kinematics and dynamics of a freely tumbling target are given by [19]

$$\dot{\boldsymbol{q}}_t = \frac{1}{2}\boldsymbol{\Omega}\left(\boldsymbol{\omega}_t\right)\boldsymbol{q}_t \tag{9}$$

$$\boldsymbol{I}_t\dot{\boldsymbol{\omega}}_t + \boldsymbol{\omega}_t \times \boldsymbol{I}_t\boldsymbol{\omega}_t = \boldsymbol{0} \tag{10}$$

where $\boldsymbol{q}_t = \left[q_{t0} \quad \boldsymbol{q}_{tv}^{\mathrm{T}}\right]^{\mathrm{T}}$ and $\boldsymbol{\omega}_t \in \mathbb{R}^3$ represent attitude quaternion and attitude angular velocity of the target from inertial frame to body-fixed frame, respectively. $\boldsymbol{q}_{tv} \in \mathbb{R}^3$ is the vector component of quaternion $\boldsymbol{q}_t$. $\boldsymbol{I}_t \in \mathbb{R}^{3\times 3}$ is the inertia moment of the target. And $\boldsymbol{\Omega}\left(\boldsymbol{\omega}_t\right)$ is defined as

$$\boldsymbol{\Omega}(\boldsymbol{\omega}_t)=\begin{bmatrix} 0 & -\boldsymbol{\omega}_t^{\mathrm{T}} \\ \boldsymbol{\omega}_t & -\boldsymbol{\omega}_t^{\times} \end{bmatrix} \tag{11}$$

where $\boldsymbol{\omega}_t^{\times}$ is the skew symmetric matrix of $\boldsymbol{\omega}_t$.

The attitude kinematics and dynamics of the servicing spacecraft are given by

$$\dot{\boldsymbol{q}}_s=\frac{1}{2}\boldsymbol{\Omega}(\boldsymbol{\omega}_s)\boldsymbol{q}_s \tag{12}$$

$$\boldsymbol{I}_s\dot{\boldsymbol{\omega}}_s+\boldsymbol{\omega}_s\times\boldsymbol{I}_s\boldsymbol{\omega}_s=\boldsymbol{T}_c+\boldsymbol{\delta} \tag{13}$$

where $\boldsymbol{q}_s=\begin{bmatrix} q_{s0} & \boldsymbol{q}_{sv}{}^{\mathrm{T}} \end{bmatrix}^{\mathrm{T}}$ and $\boldsymbol{\omega}_s\in\mathbb{R}^3$ are attitude quaternion and attitude angular velocity of the servicing spacecraft, respectively. $\boldsymbol{q}_{sv}\in\mathbb{R}^3$ is the vector component of quaternion $\boldsymbol{q}_s$. $\boldsymbol{I}_s\in\mathbb{R}^{3\times3}$ is the inertia moment of the servicing spacecraft. $\boldsymbol{T}_c\in\mathbb{R}^3$ is the control torque acting on the servicing spacecraft. $\boldsymbol{\delta}\in\mathbb{R}^3$ is the external disturbance torque acting on the servicing spacecraft.

Define the relative attitude quaternion and attitude angular velocity of the servicing spacecraft's body with respect to the target's body as $\boldsymbol{q}=\begin{bmatrix} q_0,q_1,q_2,q_3 \end{bmatrix}^{\mathrm{T}}$ and $\boldsymbol{\omega}\in\mathbb{R}^3$

$$\boldsymbol{q}=\boldsymbol{q}_t^{-1}\otimes\boldsymbol{q}_s \tag{14}$$

$$\boldsymbol{\omega}=\boldsymbol{\omega}_s-\boldsymbol{A}_{st}\boldsymbol{\omega}_t \tag{15}$$

where $\otimes$ denotes quaternion multiplication, $\boldsymbol{A}_{st}\in\mathbb{R}^{3\times3}$ is the transformation matrix from the target's body-fixed frame to the servicing spacecraft's body-fixed frame. And $\boldsymbol{q}$ satisfies the constraint $\boldsymbol{q}^{\mathrm{T}}\boldsymbol{q}=1$.

The attitude kinemics of the servicing spacecraft with respect to the target are given by

$$\dot{\boldsymbol{q}}=\frac{1}{2}\boldsymbol{\Omega}(\boldsymbol{\omega})\boldsymbol{q} \tag{16}$$

Taking the time derivative of $\boldsymbol{\omega}$ yields

$$\dot{\boldsymbol{\omega}}=\dot{\boldsymbol{\omega}}_s-\boldsymbol{A}_{st}\dot{\boldsymbol{\omega}}_t+\boldsymbol{\omega}\times\boldsymbol{A}_{st}\boldsymbol{\omega}_t \tag{17}$$

Substituting Eq. (10) and Eq. (13) into Eq. (17) yields

$$\dot{\boldsymbol{\omega}}=-\boldsymbol{I}_s^{-1}\left[\left(\boldsymbol{\omega}+\boldsymbol{A}_{st}\boldsymbol{\omega}_t\right)\times\boldsymbol{I}_s\left(\boldsymbol{\omega}+\boldsymbol{A}_{st}\boldsymbol{\omega}_t\right)\right]+\boldsymbol{\omega}\times\boldsymbol{A}_{st}\boldsymbol{\omega}_t+\boldsymbol{A}_{st}\boldsymbol{I}_t^{-1}\left(\boldsymbol{\omega}_t\times\boldsymbol{I}_t\boldsymbol{\omega}_t\right)+\boldsymbol{I}_s^{-1}\left(\boldsymbol{T}_c+\boldsymbol{\delta}\right) \tag{18}$$

The general relative position and attitude dynamics of the servicing spacecraft with respect to the target are formulated in Eq. (6), Eq. (16) and Eq. (18). In section 3, the coupled term will be introduced between the relative position and attitude, and the integrated coupled dynamics of relative position and attitude will be established for the controller design. Before investigating the integrated coupled dynamics of relative position and attitude, let's give insight into the control objective of a servicing spacecraft approaching and docking with a tumbling target.

2.3. Control Objective

In order to implement the docking operations, we must make sure that the docking port of the servicing spacecraft is always pointing to the docking port of the tumbling target. This constraint can be achieved via precise attitude synchronization and relative position tracking. In other words, the control system onboard the servicing spacecraft adjusts the servicing spacecraft's attitude and maneuvers its position such that the constraint is satisfied for docking and other service operations [19].

The control scheme is consist of two parts, one is the relative position tracking, the other is the attitude synchronization. The relative position tracking is to zero the line-of-sight angle of target, which will achieve the target's docking port point to the center of servicing spacecraft. And the attitude synchronization is to zero the line-of-sight angle of servicing spacecraft, which will make the servicing spacecraft's docking port point to the center of target. Thus, the two parts will together make the servicing spacecraft approach target along the line-of-sight. As a result, the control objective is achieved. And, the detail of the two parts' objective will be described as follows.

The objective of the relative position tracking is to drive the servicing spacecraft to a safe constant distance away from the target and maintain it at the safe constant distance. The desired relative position vector and the desired constant relative distance are defined as $\boldsymbol{\rho}_d \in \mathbb{R}^3$ and r_d, respectively. Thus, the desired relative position vector is expressed as

$$\boldsymbol{\rho}_d = \boldsymbol{A}_{Lt}\boldsymbol{r}_d \tag{19}$$

where $\boldsymbol{r}_d = \begin{bmatrix} r_d & 0 & 0 \end{bmatrix}^{\mathrm{T}}$, $\boldsymbol{A}_{Lt} \in \mathbb{R}^{3\times 3}$ is the transformation matrix from the target's body-fixed frame to the LVLH frame.

Eq. (19) shows that the desired relative position vector $\boldsymbol{\rho}_d$ is a time-varying quantity and its direction in space depends upon the attitude of the target. Therefore, the objective of the relative position tracking is to ensure that $\boldsymbol{\rho}_L \to \boldsymbol{A}_{Lt}\boldsymbol{\rho}_d$.

The objective of the attitude synchronization is to find the appropriate torque input to eliminate the error between the desired orientation of the servicing spacecraft's docking port and the current orientation. According to the direction definition of the docking port of the servicing spacecraft and the target, we'll get that the desired attitude of the servicing spacecraft is the same as the attitude of the target. Therefore, the objective of the attitude synchronization is to ensure the relative attitude quaternion $\boldsymbol{q} \to \begin{bmatrix} 1,0,0,0 \end{bmatrix}^{\mathrm{T}}$. Note that since the target is uncontrolled and tumbles freely, the direction of the target's docking port changes as well. Hence, the desired orientation of the servicing spacecraft's docking port changes as well.

3. Integrated Coupled Dynamics of Relative Position and Attitude

It's a well-known fact that the relative position and attitude dynamics is coupled for the reason that the orbit thrusters are fixed in the body-fixed frame of servicing spacecraft. In order to design the integrated coupled controller, the integrated coupled dynamics of the relative position and attitude are necessary to investigate.

To model the integrated coupled dynamics, the attitude matrix related to the servicing spacecraft's attitude and the target's attitude is introduced into the relative position dynamic equations. And, the relative attitude dynamic equations expressed in

two-order differential form of quaternion are derived. Thus, the integrated coupled dynamics is established to design the integrated coupled control law for relative position and attitude.

Since the servicing spacecraft's thrusters are fixed along its body frame, the thrust acceleration should meet the following relationship

$$\boldsymbol{a}_L = \boldsymbol{A}_{Ls}\boldsymbol{a}_b \tag{20}$$

$$\boldsymbol{A}_{Ls} = \boldsymbol{A}_{LI}\boldsymbol{A}_{tI}^{\mathrm{T}}\boldsymbol{A}_{st}^{\mathrm{T}} \tag{21}$$

where $\boldsymbol{a}_b \in \mathbb{R}^3$ is the thrust acceleration expressed in the servicing spacecraft's body-fixed frame. $\boldsymbol{A}_{Ls} \in \mathbb{R}^{3\times3}$ is the transformation matrix from the servicing spacecraft's body-fixed frame to the LVLH frame. $\boldsymbol{A}_{LI} \in \mathbb{R}^{3\times3}$ is the transformation matrix from the Earth-centered inertial frame to the LVLH frame. $\boldsymbol{A}_{tI} \in \mathbb{R}^{3\times3}$ is the transformation matrix from the Earth-centered inertial frame to the target's body-fixed frame.

Substituting Eq. (20) into Eq. (6) yields the relative position dynamics, in the LVLH frame, of the servicing spacecraft with respect to the target is described as

$$\ddot{\boldsymbol{\rho}}_L + \boldsymbol{A}_2\dot{\boldsymbol{\rho}}_L + \boldsymbol{A}_1\boldsymbol{\rho}_L = \boldsymbol{A}_{Ls}\boldsymbol{a}_b + \boldsymbol{f}_L \tag{22}$$

where $\boldsymbol{A}_{Ls}$ implies the dynamics coupling between the relative position and attitude.

Taking the time derivative of Eq. (16), and applying Eq. (18) yields the relative attitude dynamic equations expressed as

$$\begin{bmatrix}\ddot{q}_0\\ \ddot{\boldsymbol{q}}_v\end{bmatrix} = \begin{bmatrix}-\frac{1}{4}\left(\boldsymbol{\omega}^{\mathrm{T}}(\boldsymbol{q},\dot{\boldsymbol{q}})\boldsymbol{\omega}(\boldsymbol{q},\dot{\boldsymbol{q}})\right)q_0 - \frac{1}{2}\boldsymbol{q}_v^{\mathrm{T}}\boldsymbol{f}(\boldsymbol{q},\dot{\boldsymbol{q}},\boldsymbol{\omega}_t)\\ -\frac{1}{4}\left(\boldsymbol{\omega}^{\mathrm{T}}(\boldsymbol{q},\dot{\boldsymbol{q}})\boldsymbol{\omega}(\boldsymbol{q},\dot{\boldsymbol{q}})\right)\boldsymbol{q}_v + \frac{1}{2}\boldsymbol{Q}_v\boldsymbol{f}(\boldsymbol{q},\dot{\boldsymbol{q}},\boldsymbol{\omega}_t)\end{bmatrix} + \begin{bmatrix}-\frac{1}{2}\boldsymbol{q}_v^{\mathrm{T}}\boldsymbol{I}_s^{-1}(\boldsymbol{T}_c+\boldsymbol{\delta})\\ \frac{1}{2}\boldsymbol{Q}_v\boldsymbol{I}_s^{-1}(\boldsymbol{T}_c+\boldsymbol{\delta})\end{bmatrix} \tag{23}$$

where $\boldsymbol{q}_v = [q_1, q_2, q_3]^{\mathrm{T}}$ is the vector component of relative attitude quaternion $\boldsymbol{q}$, and

$$\boldsymbol{Q}_v = \begin{bmatrix} q_0 & -q_3 & q_2\\ q_3 & q_0 & -q_1\\ -q_2 & q_1 & q_0\end{bmatrix} \tag{24}$$

$$\boldsymbol{\omega}(\boldsymbol{q},\dot{\boldsymbol{q}}) = \begin{bmatrix}\omega_x\\ \omega_y\\ \omega_z\end{bmatrix} = \begin{bmatrix}2(q_0\dot{q}_1 + q_3\dot{q}_2 - q_2\dot{q}_3 - q_1\dot{q}_0)\\ 2(q_0\dot{q}_2 + q_1\dot{q}_3 - q_3\dot{q}_1 - q_2\dot{q}_0)\\ 2(q_0\dot{q}_3 + q_2\dot{q}_1 - q_1\dot{q}_2 - q_3\dot{q}_0)\end{bmatrix} \tag{25}$$

$$\begin{aligned}\boldsymbol{f}(\boldsymbol{q},\dot{\boldsymbol{q}},\boldsymbol{\omega}_t) = &-\boldsymbol{I}_s^{-1}\left[\left(\boldsymbol{\omega}(\boldsymbol{q},\dot{\boldsymbol{q}}) + \boldsymbol{A}_{st}\boldsymbol{\omega}_t\right)\times\boldsymbol{I}_s\left(\boldsymbol{\omega}(\boldsymbol{q},\dot{\boldsymbol{q}}) + \boldsymbol{A}_{st}\boldsymbol{\omega}_t\right)\right]\\ &+\boldsymbol{\omega}(\boldsymbol{q},\dot{\boldsymbol{q}})\times\boldsymbol{A}_{st}\boldsymbol{\omega}_t + \boldsymbol{A}_{st}\boldsymbol{I}_t^{-1}\left(\boldsymbol{\omega}_t\times\boldsymbol{I}_t\boldsymbol{\omega}_t\right)\end{aligned} \tag{26}$$

Due to the normalization constraint of quaternion, for attitude control, it only needs to control the vector component of quaternion. The dynamic equations of the vector component of relative quaternion can be expressed as

$$\ddot{\boldsymbol{q}}_v = \boldsymbol{f}_v + \boldsymbol{G}(\boldsymbol{T}_c + \boldsymbol{\delta}) \tag{27}$$

where

$$\boldsymbol{f}_v = -\frac{1}{4}\left(\boldsymbol{\omega}^{\mathrm{T}}(\boldsymbol{q},\dot{\boldsymbol{q}})\boldsymbol{\omega}(\boldsymbol{q},\dot{\boldsymbol{q}})\right)\boldsymbol{q}_v + \frac{1}{2}\boldsymbol{Q}_v \boldsymbol{f}(\boldsymbol{q},\dot{\boldsymbol{q}},\boldsymbol{\omega}_t) \tag{28}$$

$$\boldsymbol{G} = \frac{1}{2}\boldsymbol{Q}_v \boldsymbol{I}_s^{-1} \tag{29}$$

Taking as sate variables $\boldsymbol{x} = \left[\boldsymbol{\rho}_L^{\mathrm{T}}, \boldsymbol{q}_v^{\mathrm{T}}\right]^{\mathrm{T}}$, thus, the integrated coupled dynamics of relative position and attitude can be described as

$$\ddot{\boldsymbol{x}} = \boldsymbol{f}(\boldsymbol{x},\dot{\boldsymbol{x}}) + \boldsymbol{B}\boldsymbol{u} + \boldsymbol{D}\boldsymbol{d} \tag{30}$$

where

$$\boldsymbol{f}(\boldsymbol{x},\dot{\boldsymbol{x}}) = \begin{bmatrix} -\boldsymbol{A}_2\dot{\boldsymbol{\rho}}_L - \boldsymbol{A}_1\boldsymbol{\rho}_L \\ \boldsymbol{f}_v \end{bmatrix} \tag{31}$$

$$\boldsymbol{u} = \left[\boldsymbol{a}_b^{\mathrm{T}}, \boldsymbol{T}_c^{\mathrm{T}}\right]^{\mathrm{T}}, \quad \boldsymbol{d} = \left[\boldsymbol{f}_L^{\mathrm{T}}, \boldsymbol{\delta}^{\mathrm{T}}\right]^{\mathrm{T}} \tag{32}$$

$$\boldsymbol{B} = \begin{bmatrix} \boldsymbol{A}_{Ls} & \boldsymbol{0}_{3\times3} \\ \boldsymbol{0}_{3\times3} & \boldsymbol{G} \end{bmatrix}, \quad \boldsymbol{D} = \begin{bmatrix} \boldsymbol{I}_{3\times3} & \boldsymbol{0}_{3\times3} \\ \boldsymbol{0}_{3\times3} & \boldsymbol{G} \end{bmatrix} \tag{33}$$

The desired state is defined as $\boldsymbol{x}_d = \left[\left(\boldsymbol{A}_{Lt}\boldsymbol{\rho}_d\right)^{\mathrm{T}}, \boldsymbol{0}_{1\times3}\right]^{\mathrm{T}}$, and the objective of the integrated coupled control of relative position and attitude is to find the appropriate force and torque input to eliminate the error between the desired state $\boldsymbol{x}_d$ and the current state $\boldsymbol{x}$. In other words, the objective of the integrated control law is to ensure that $\boldsymbol{x} \to \boldsymbol{x}_d$.

4. Integrated Coupled Control Law Design

In this section, the integrated coupled control law, for relative position and attitude of proximity maneuvering, will be explicitly discussed. And the integrated coupled control law is presented through a new robust sliding mode control technique, which shows effective performance to overcome the unknown but bounded disturbances and model uncertainties. The new robust sliding mode control technique is obtained using a method which consists of two sliding surfaces. The first sliding surface is constructed by the state error and the state error rate, and the second sliding surface is designed by integrating the sign function of the first sliding surface. Note that the second sliding surface is used to automatically compensate the external disturbances without the need to explicitly estimate it.

Now, the integrated coupled control law is designed in detail as follows.

4.1. Sliding Surfaces Design

Taking as the first sliding surface

$$\boldsymbol{s} = \dot{\boldsymbol{e}} + \boldsymbol{k}\boldsymbol{e} \tag{34}$$

where $\boldsymbol{k} \in \mathbb{R}^{6\times6}$ is positive diagonal matrix, $\boldsymbol{e} \in \mathbb{R}^{6}$ is the error between the current state and the desired state described as

$$\boldsymbol{e} = \boldsymbol{x} - \boldsymbol{x}_d = \begin{bmatrix} \boldsymbol{\rho}_L - \boldsymbol{A}_{Lt}\boldsymbol{r}_d \\ \boldsymbol{q}_v \end{bmatrix} \tag{35}$$

The error rate $\dot{\boldsymbol{e}} \in \mathbb{R}^6$ can be obtained through taking the time derivative of Eq. (35)

$$\dot{\boldsymbol{e}} = \dot{\boldsymbol{x}} - \dot{\boldsymbol{x}}_d = \begin{bmatrix} \dot{\boldsymbol{\rho}}_L - \boldsymbol{A}_{Lt}\left(\boldsymbol{\omega}_{Lt} \times \boldsymbol{r}_d\right) \\ \dot{\boldsymbol{q}}_v \end{bmatrix} \tag{36}$$

where

$$\boldsymbol{\omega}_{Lt} = \boldsymbol{\omega}_t - \boldsymbol{A}_{Lt}{}^{\mathrm{T}}\boldsymbol{\omega}_L \tag{37}$$

and $\boldsymbol{\omega}_L \in \mathbb{R}^3$ is the rotation angular velocity of the LVLH frame with respect to the Earth-centred inertial frame. $\boldsymbol{\omega}_{Lt} \in \mathbb{R}^3$ is the rotation angular velocity of the target's body-fixed frame with respect to the LVLH frame.

Taking the time derivative of Eq. (36) yields

$$\ddot{\boldsymbol{e}} = \ddot{\boldsymbol{x}} - \ddot{\boldsymbol{x}}_d = \begin{bmatrix} \ddot{\boldsymbol{\rho}}_L - \boldsymbol{A}_{Lt}\left[\dot{\boldsymbol{\omega}}_{Lt} \times \boldsymbol{\rho}_d + \boldsymbol{\omega}_{Lt} \times \left(\boldsymbol{\omega}_{Lt} \times \boldsymbol{\rho}_d\right)\right] \\ \ddot{\boldsymbol{q}}_v \end{bmatrix} \tag{38}$$

where

$$\dot{\boldsymbol{\omega}}_{Lt} = \dot{\boldsymbol{\omega}}_t - \boldsymbol{A}_{Lt}{}^{\mathrm{T}}\dot{\boldsymbol{\omega}}_L + \boldsymbol{\omega}_{Lt} \times \left(\boldsymbol{A}_{Lt}{}^{\mathrm{T}}\boldsymbol{\omega}_L\right) \tag{39}$$

where $\boldsymbol{\omega}_L = \begin{bmatrix} 0 & 0 & \dot{\theta} \end{bmatrix}^{\mathrm{T}}$, $\dot{\boldsymbol{\omega}}_L = \begin{bmatrix} 0 & 0 & -2\dot{R}_T\dot{\theta}/R_T \end{bmatrix}^{\mathrm{T}}$.

Substituting Eq. (30) into Eq. (38) yields

$$\ddot{\boldsymbol{e}} = \ddot{\boldsymbol{x}} - \boldsymbol{f}(\boldsymbol{\omega}_{Lt}) \tag{40}$$

where

$$\boldsymbol{f}\left(\boldsymbol{\omega}_{Lt}\right) = \begin{bmatrix} \boldsymbol{A}_{Lt}\left[\dot{\boldsymbol{\omega}}_{Lt} \times \boldsymbol{\rho}_d + \boldsymbol{\omega}_{Lt} \times \left(\boldsymbol{\omega}_{Lt} \times \boldsymbol{\rho}_d\right)\right] \\ \boldsymbol{0}_{3\times 1} \end{bmatrix} \tag{41}$$

Taking the time derivative of Eq. (34) obtains

$$\dot{\boldsymbol{s}} = \ddot{\boldsymbol{e}} + \boldsymbol{k}\dot{\boldsymbol{e}} = \ddot{\boldsymbol{x}} - \boldsymbol{f}(\boldsymbol{\omega}_{Lt}) + \boldsymbol{k}\left(\dot{\boldsymbol{x}} - \dot{\boldsymbol{x}}_d\right) \tag{42}$$

The second sliding surface is designed as

$$\boldsymbol{\eta} = \boldsymbol{s} + k_0 \int_0^t \mathrm{sign}\left(\boldsymbol{s}\right) d\tau \tag{43}$$

where $k_0 > 0$.

Taking the time derivative of Eq. (43) leads to

$$\dot{\boldsymbol{\eta}} = k_0 \mathrm{sign}\left(\boldsymbol{s}\right) + \dot{\boldsymbol{s}} \tag{44}$$

In order to guarantee that the sliding surface will be achieved in finite time, the sliding mode control design must meet the following Lemma [27, 28]

Lemma The origin of a differential equation

$$\dot{z} = -\beta z^b \text{ , } z(0) > 0 \text{ , } \beta > 0 \tag{45}$$

is a terminal attractor with a finite reaching time

$$t_r = \frac{\left(z(0)\right)^{1-b}}{\beta(1-b)}, \forall b \in (0,1) \tag{46}$$

Indeed, integrating Equation(45) to obtain

$$\left(z(t)\right)^{1-b} = \left(z(0)\right)^{1-b} - \beta(1-b)t \tag{47}$$

Requiring $z(t_r)=0$ implies formula Eq.(46). Similarly, if $\dot{z} \le -\beta z^b$, then $t_r \le \frac{\left(z(0)\right)^{1-b}}{\beta(1-b)}$.

So, a candidate Lyapunov function and its derivative are constructed as

$$V = \frac{1}{2}\boldsymbol{\eta}^{\mathrm{T}}\boldsymbol{\eta} \tag{48}$$

and

$$\dot{V} = \boldsymbol{\eta}^{\mathrm{T}}\dot{\boldsymbol{\eta}} \le -\beta V^b \tag{49}$$

where $0 < b < 1$, $\beta > 0$.

4.2. Robust Sliding Mode Control Law

The sliding mode control law is designed as

$$\boldsymbol{u} = -\boldsymbol{u}_e - \boldsymbol{u}_d \tag{50}$$

where $\boldsymbol{u}_e \in \mathbb{R}^6$ is the equivalent control that governs the sliding motion of the system, and $\boldsymbol{u}_d \in \mathbb{R}^6$ is the control function that governs the motion of reaching to the sliding surface.

Substituting Eq. (42) into Eq. (44), and applying Eq. (30) and Eq. (50) obtains the following equation

$$\dot{\boldsymbol{\eta}} = k_0 \mathrm{sign}(\boldsymbol{s}) + \boldsymbol{f}(\boldsymbol{x}, \dot{\boldsymbol{x}}) - \boldsymbol{f}(\boldsymbol{\omega}_{Lt}) + \boldsymbol{k}(\dot{\boldsymbol{x}} - \dot{\boldsymbol{x}}_d) - \boldsymbol{B}\boldsymbol{u}_e - \boldsymbol{B}\boldsymbol{u}_d + \boldsymbol{D}\boldsymbol{d} \tag{51}$$

Setting $\dot{\boldsymbol{\eta}} = \boldsymbol{0}$ and $\boldsymbol{u}_d = \boldsymbol{0}$. Since the rank of matrix $\boldsymbol{B}$ is full, the inverse of matrix $\boldsymbol{B}$ exits. Therefore, solving Eq. (51), it leads to the equivalent control

$$\boldsymbol{u}_e = \boldsymbol{B}^{-1}\left[k_0 \mathrm{sign}(\boldsymbol{s}) + \boldsymbol{f}(\boldsymbol{x}, \dot{\boldsymbol{x}}) - \boldsymbol{f}(\boldsymbol{\omega}_{Lt}) + \boldsymbol{k}(\dot{\boldsymbol{x}} - \dot{\boldsymbol{x}}_d) + \boldsymbol{D}\boldsymbol{d}\right] \tag{52}$$

It's a well-known fact that it is very hard, in general, to obtain the exact value of unknown disturbances $\boldsymbol{D}\boldsymbol{d}$. And, the value of $\boldsymbol{x}$ and $\dot{\boldsymbol{x}}$ cannot be exactly measured or determined. Thus, $\boldsymbol{u}_e$ cannot be exactly measured or determined. Therefore, $\hat{\boldsymbol{u}}_e$ which is the best estimate of $\boldsymbol{u}_e$, is given by

$$\hat{\boldsymbol{u}}_e = \hat{\boldsymbol{B}}^{-1}\left[k_0 \mathrm{sign}(\hat{\boldsymbol{s}}) + \boldsymbol{f}(\hat{\boldsymbol{x}}, \hat{\dot{\boldsymbol{x}}}) - \boldsymbol{f}(\hat{\boldsymbol{\omega}}_{Lt}) + \boldsymbol{k}(\hat{\dot{\boldsymbol{x}}} - \hat{\dot{\boldsymbol{x}}}_d)\right] \tag{53}$$

where $\hat{\boldsymbol{m}}$ denotes the estimated or measured value of the exact value $\boldsymbol{m}$.

The sliding mode control law is still effective as long as the error between the true value and the estimated value is bounded by

$$\left\| \boldsymbol{B}\boldsymbol{u}_e - \boldsymbol{B}\hat{\boldsymbol{u}}_e \right\|_2 \le d_0 \tag{54}$$

where $d_0 > 0$.

Applying this to the derivative of the Lyapunov function of Eq. (49) obtains the following inequality

$$\begin{aligned} \dot{V} &= \boldsymbol{\eta}^{\mathrm{T}}\dot{\boldsymbol{\eta}} = \boldsymbol{\eta}^{\mathrm{T}}\left(\boldsymbol{B}\boldsymbol{u}_e - \boldsymbol{B}\hat{\boldsymbol{u}}_e - \boldsymbol{B}\boldsymbol{u}_d\right) \\ &\le \left\|\boldsymbol{\eta}\right\|_2 \left\|\boldsymbol{B}\boldsymbol{u}_e - \boldsymbol{B}\hat{\boldsymbol{u}}_e\right\|_2 - \boldsymbol{\eta}^{\mathrm{T}}\boldsymbol{B}\boldsymbol{u}_d \\ &\le \left\|\boldsymbol{\eta}\right\|_2 d_0 - \boldsymbol{\eta}^{\mathrm{T}}\boldsymbol{B}\boldsymbol{u}_d \end{aligned} \tag{55}$$

According to the finite reaching time condition, the following inequality should be satisfied

$$\left\|\boldsymbol{\eta}\right\|_2 d_0 - \boldsymbol{\eta}^{\mathrm{T}}\boldsymbol{B}\boldsymbol{u}_d \le -\frac{\beta}{2^b}\left\|\boldsymbol{\eta}\right\|_2^{2b} \tag{56}$$

In order to meet the inequality of Eq. (56), the control $\boldsymbol{u}_d$, is designed as

$$\boldsymbol{u}_d = \boldsymbol{B}^{-1}\frac{\boldsymbol{\lambda}}{2^b}\left\|\boldsymbol{\eta}\right\|_2^{2b-1}\operatorname{sign}(\boldsymbol{\eta}) \tag{57}$$

where $\boldsymbol{\lambda} \in \mathbb{R}^{6\times 6}$ is positive diagonal matrix, and $0.5 < b < 1$.

Assuming that γ_1 and γ_2 are the minimum eigenvalue and maximum eigenvalue of $\boldsymbol{\lambda}$, respectively. Substituting Eq. (57) into Eq. (56), and after simplifying, we obtains

$$\left\|\boldsymbol{\eta}\right\|_2 \ge \left(2^b \frac{d_0}{\gamma_1 - \beta}\right)^{\frac{1}{2b-1}} = \mathrm{ROC} \tag{58}$$

This means that $V > 0$ for $\boldsymbol{\eta} \ne 0$ and $\dot{V} \le -\frac{\beta}{2^b}\left\|\boldsymbol{\eta}\right\|_2^{2b}$ for $\left\|\boldsymbol{\eta}\right\|_2 \ge \left(2^b \frac{d_0}{\gamma_1 - \beta}\right)^{\frac{1}{2b-1}}$. Therefore, the second sliding surface $\boldsymbol{\eta}$ will converge to ROC in finite time. And, the ROC can be made arbitrarily small by selecting $0 < 2^b \frac{d_0}{\gamma_1 - \beta} = \bar{\varepsilon} < 1$ as the result of $\frac{1}{2b-1} > 1$. This leads to the selection of γ_1 as

$$\gamma_1 > 2^b d_0 + \beta \tag{59}$$

or

$$\gamma_1 = \frac{2^b}{\bar{\varepsilon}} d_0 + \beta \tag{60}$$

Two norm of the time derivative of the second sliding surface $\boldsymbol{\eta}$ is described as

$$\begin{aligned} \left\|\dot{\boldsymbol{\eta}}\right\|_2 &= \left\|\boldsymbol{B}\boldsymbol{u}_e - \boldsymbol{B}\hat{\boldsymbol{u}}_e - \boldsymbol{B}\boldsymbol{u}_d\right\|_2 \\ &\le \left\|\boldsymbol{B}\boldsymbol{u}_e - \boldsymbol{B}\hat{\boldsymbol{u}}_e\right\|_2 + \left\|\boldsymbol{B}\boldsymbol{u}_d\right\|_2 \\ &\le d_0 + \frac{3\gamma_2}{2^{b-1}}\left\|\boldsymbol{\eta}\right\|_2^{2b-1} \end{aligned} \tag{61}$$

Note that $\left\|\dot{\boldsymbol{\eta}}\right\|_2$ will converge to $\frac{6\gamma_2 d_0}{\gamma_1 - \beta} + d_0$ in finite time, as the result of $\left\|\boldsymbol{\eta}\right\|_2$ will converge to

$\left(2^b \frac{d_0}{\gamma_1 - \beta}\right)^{\frac{1}{2b-1}}$ in finite time.

As a matter of fact, the exact value of $\boldsymbol{u}_d$ can not be obtained, $\hat{\boldsymbol{u}}_d$, which is the best estimate value of $\boldsymbol{u}_d$, is given by

$$\hat{\boldsymbol{u}}_d = \hat{\boldsymbol{B}}^{-1} \frac{\boldsymbol{\lambda}}{2^b} \|\hat{\boldsymbol{\eta}}\|_2^{2b-1} \operatorname{sign}(\hat{\boldsymbol{\eta}}) \tag{62}$$

and assuming that $\boldsymbol{u}_d = \hat{\boldsymbol{u}}_d + \boldsymbol{u}_t$, where $\boldsymbol{u}_t$ is the error between the true value and the estimated value of $\boldsymbol{u}_d$. The sliding mode control law is still effective as long as the error $\boldsymbol{u}_t$ is bounded by

$$\|\boldsymbol{B}\boldsymbol{u}_d - \boldsymbol{B}\hat{\boldsymbol{u}}_d\|_2 = \|\boldsymbol{B}\boldsymbol{u}_t\|_2 \le d_1 \tag{63}$$

where $d_1 > 0$.

The derivative of the Lyapunov function of Eq. (49) obtains the following inequality

$$\begin{aligned} \dot{V} &= \boldsymbol{\eta}^{\mathrm{T}} \dot{\boldsymbol{\eta}} = \boldsymbol{\eta}^{\mathrm{T}} \left(\boldsymbol{B}\boldsymbol{u}_e - \boldsymbol{B}\hat{\boldsymbol{u}}_e - \boldsymbol{B}\hat{\boldsymbol{u}}_d\right) \\ &\le \|\boldsymbol{\eta}\|_2 \|\boldsymbol{B}\boldsymbol{u}_e - \boldsymbol{B}\hat{\boldsymbol{u}}_e\|_2 + \|\boldsymbol{\eta}\|_2 \|\boldsymbol{B}\boldsymbol{u}_t\|_2 - \boldsymbol{\eta}^{\mathrm{T}} \boldsymbol{B}\boldsymbol{u}_d \\ &\le \|\boldsymbol{\eta}\|_2 \left(d_0 + d_1\right) - \boldsymbol{\eta}^{\mathrm{T}} \boldsymbol{B}\boldsymbol{u}_d \end{aligned} \tag{64}$$

So, $\dot{V} \le -\frac{\beta}{2^b} \|\boldsymbol{\eta}\|_2^{2b}$ for $\|\boldsymbol{\eta}\|_2 \ge \left(2^b \frac{d_0 + d_1}{\gamma_1 - \beta}\right)^{\frac{1}{2b-1}}$, the selection of γ_1 should be

$$\gamma_1 > 2^b \left(d_0 + d_1\right) + \beta \tag{65}$$

In this case, $\|\dot{\boldsymbol{\eta}}\|_2$ is described as

$$\begin{aligned} \|\dot{\boldsymbol{\eta}}\|_2 &= \|\boldsymbol{B}\boldsymbol{u}_e - \boldsymbol{B}\hat{\boldsymbol{u}}_e - \boldsymbol{B}\hat{\boldsymbol{u}}_d\|_2 \\ &\le \|\boldsymbol{B}\boldsymbol{u}_e - \boldsymbol{B}\hat{\boldsymbol{u}}_e\|_2 + \|\boldsymbol{B}\boldsymbol{u}_t\|_2 + \|\boldsymbol{B}\boldsymbol{u}_d\|_2 \\ &\le d_0 + d_1 + \frac{3\gamma_2}{2^{b-1}} \|\boldsymbol{\eta}\|_2^{2b-1} \end{aligned} \tag{66}$$

Therefore, $\|\dot{\boldsymbol{\eta}}\|_2$ will converge to $\frac{6\gamma_2 \left(d_0 + d_1\right)}{\gamma_1 - \beta} + d_0 + d_1$ in finite time.

Now, let's give insight into the convergence of $\boldsymbol{s}$, a candidate Lyapunov function and its derivative are constructed as

$$V = \frac{1}{2} \boldsymbol{s}^{\mathrm{T}} \boldsymbol{s} \tag{67}$$

and

$$\begin{aligned} \dot{V} &= \boldsymbol{s}^{\mathrm{T}} \dot{\boldsymbol{s}} \\ &= \boldsymbol{s}^{\mathrm{T}} \left[\dot{\boldsymbol{\eta}} - k_0 \operatorname{sign}\left(\boldsymbol{s}\right)\right] \\ &\le \|\boldsymbol{s}\|_2 \left(\|\dot{\boldsymbol{\eta}}\|_2 - k_0\right) \end{aligned} \tag{68}$$

According to the **Lemma**, in order to guarantee that reaching to the first sliding surface $\boldsymbol{s}$ in finite time, the following inequality should be satisfied [28]

$$\|\boldsymbol{s}\|_2 \left(\|\dot{\boldsymbol{\eta}}\|_2 - k_0\right) \le -\frac{\zeta}{\sqrt{2}}\|\boldsymbol{s}\|_2 \tag{69}$$

where $\zeta > 0$.

This also means that if Eq. (69) is satisfied, the first sliding surface s will converge to zero in finite time. In order to meet the inequality Eq. (69), the selection of k_0 should satisfy the following inequality

$$k_0 \ge \frac{6\gamma_2 (d_0 + d_1)}{\gamma_1 - \beta} + d_0 + d_1 + \frac{\zeta}{\sqrt{2}} \tag{70}$$

Let's give insight into the convergence of the system state. After reaching the first sliding surface, $\boldsymbol{s} = \boldsymbol{0}$, this means that $\dot{\boldsymbol{e}} = -\boldsymbol{k}\boldsymbol{e}$, solving this equation, we know that the state error $\boldsymbol{e}$ will exponentially converge to zero. And, $\dot{\boldsymbol{e}}$ will converge to zero as $\boldsymbol{e}$ converges to zero. This means that $\boldsymbol{x}$ will converge to $\boldsymbol{x}_d$, and $\dot{\boldsymbol{x}}$ will converge to $\dot{\boldsymbol{x}}_d$.

So, the final integrated coupled control law is described as

$$\boldsymbol{u} = -\hat{\boldsymbol{B}}^{-1}\left[k_0 \operatorname{sign}(\hat{\boldsymbol{s}}) + \boldsymbol{f}(\hat{\boldsymbol{x}}, \hat{\dot{\boldsymbol{x}}}) - \boldsymbol{f}(\hat{\boldsymbol{\omega}}_{Lt}) + \boldsymbol{k}\left(\hat{\dot{\boldsymbol{x}}} - \hat{\dot{\boldsymbol{x}}}_d\right)\right] - \hat{\boldsymbol{B}}^{-1}\frac{\boldsymbol{\lambda}}{2^b}\|\hat{\boldsymbol{\eta}}\|_2^{2b-1}\operatorname{sign}(\hat{\boldsymbol{\eta}}) \tag{71}$$

4.3. Robustness to Measurement Noise

The convergence of the sliding surface will change when the measurement noise exits. It's necessary to consider the effects of stochastic noise on the system. In this case, noise is added to the state error and state error rate as

$$\begin{aligned} \tilde{\boldsymbol{e}} &= \boldsymbol{e} + \boldsymbol{v}_1 \\ \dot{\tilde{\boldsymbol{e}}} &= \dot{\boldsymbol{e}} + \boldsymbol{v}_2 \end{aligned} \tag{72}$$

where $\boldsymbol{v}_1 \in \mathbb{R}^6$ and $\boldsymbol{v}_2 \in \mathbb{R}^6$ are noises which are bounded by

$$\|\boldsymbol{v}_1\|_2 \le \alpha_1, \|\boldsymbol{v}_2\|_2 \le \alpha_2 \tag{73}$$

where $\alpha_1 > 0$, $\alpha_2 > 0$.

Applying Eq. (34), the first sliding surface with measurement noise is described as

$$\tilde{\boldsymbol{s}} = \boldsymbol{s} + \boldsymbol{v}_3 \tag{74}$$

where $\boldsymbol{v}_3 \in \mathbb{R}^6$, and $\boldsymbol{v}_3 = \boldsymbol{k}\boldsymbol{v}_1 + \boldsymbol{v}_2$, which is bounded by

$$\|\boldsymbol{v}_3\|_2 \le 6\gamma_3\alpha_1 + \alpha_2 = \alpha_3 \tag{75}$$

where γ_3 denotes the maximum eigenvalue of matrix $\boldsymbol{k}$.

Assuming that $|s_i| > |v_{3i}|$ for i=1,2,3,4,5,6 during the reaching phase, then $\operatorname{sign}(\tilde{\boldsymbol{s}}) = \operatorname{sign}(\boldsymbol{s} + \boldsymbol{v}_3) = \operatorname{sign}(\boldsymbol{s})$. Therefore, in this case, the system will not converge to $\|\tilde{\boldsymbol{s}}\|_2 = 0$, but instead to

$$\|\tilde{\boldsymbol{s}}\|_2 = \|\boldsymbol{s} + \boldsymbol{v}_3\|_2 \le \|\boldsymbol{s}\|_2 + \|\boldsymbol{v}_3\|_2 \le \alpha_3 \tag{76}$$

This equation shows that the first sliding surface with measurement noise will converge to α_3 in finite time.

Using Eq. (43) leads to the second sliding surface with measurement noise, during the reaching phase, is given by

$$\tilde{\boldsymbol{\eta}} = \boldsymbol{\eta} + \boldsymbol{v}_3 \tag{77}$$

Assuming that $|\eta_i| > |v_{3i}|$ for i=1,2,3,4,5,6 during the reaching phase, then $\text{sign}(\tilde{\boldsymbol{\eta}})=\text{sign}(\boldsymbol{\eta}+\boldsymbol{v}_3)=\text{sign}(\boldsymbol{\eta})$. And the convergence of $\|\tilde{\boldsymbol{\eta}}\|_2$ is

$$\|\tilde{\boldsymbol{\eta}}\|_2 = \|\boldsymbol{\eta}+\boldsymbol{v}_3\|_2 \le \|\boldsymbol{\eta}\|_2 + \|\boldsymbol{v}_3\|_2 \to \left(2^b \frac{d_0+d_1}{\gamma_1-\beta}\right)^{\frac{1}{2b-1}} + \alpha_3 \tag{78}$$

Eq. (72) and Eq. (73) show that the state error $\tilde{\boldsymbol{e}}$ will converge to α_1, and the state error rate $\dot{\tilde{\boldsymbol{e}}}$ will converge to α_2.

4.4. Chattering and Control Constraints Problem

As we know, the chattering phenomenon is the main problem of applying the sliding mode control. However, fortunately, chattering elimination or chattering attenuation has been investigated a lot, and there are several methods to solve the chattering problem. One method is called the boundary layer method, which eliminates the chattering in the system by establishing a boundary layer around the sliding surface. This method makes the motion of the system remain within the boundary after reaching the boundary, so it eliminates the finite reaching time of the system to the sliding surface. Another method is to pass the output of the discontinuous control part through a low pass filter of an appropriate order to smooth the control signal. A similar approach is described in [29, 30], which is to pass the discontinuous control part through an artificial integrator, this method provides a continuous control to the system. However, adding additional integrators result in chattering attenuation instead of chattering elimination, while providing the appropriate level of smoothness.

The most common method of smoothing the control function is to replace the discontinuous sign function with a continuous approximation. There are several methods to accomplish that, the sign function is generally replaced with the saturation function. The saturation function can provide continuous control and eliminate chattering. Here, in order to eliminate chattering, the saturation function is used.

Since the maximum output of actuators is limited, in order to guarantee the tracking performance of the control system, the control function should be processed before introducing into the actuators. Here, the vector limiting method proposed by Wie and Lu[21] was used.

5. Numerical Simulations and Results Analysis

In this section, three numerical simulation scenarios are presented to verify the performance of the proposed control law above. Scenario 1 is to investigate the effectiveness of the control law, scenario 2 and 3 are to investigate the robustness of the control law to model uncertainties which including parameter uncertainties and unmodeled component. Note that the focus of this work here is to validate the effectiveness of the integrated coupled control law. So, no specific actuator is assumed, and the actuator dynamics is not considered in the simulation except for the maximum output of the control accelerations and control torques.

In order to avoid the collision, capture without missing, and enhance the safety and reliability of the on-orbit servicing mission, the approaching process is designed as two phases. The first phase is to drive the servicing spacecraft to a safe constant distance from the target ($r_d = 10$), which is a little larger than the final distance, and to eliminate the relative attitude error at the same time. The second phase is to drive the servicing spacecraft to the final rendezvous distance ($r_d = 5$), then, docking or other servicing operations can be done. Except for safety, this approaching strategy also makes sure that the servicing spacecraft's docking port has pointed to the target's docking port during close rendezvous and docking.

The relative perturbation acceleration is $[2.5, 4.5, 3.6]^{\mathrm{T}} \times 10^{-5} \mathrm{m/s}^2$. The measurement accuracy of relative position and velocity are 1×10^{-3}m (3σ), 1×10^{-4}m/s (3σ), respectively. The measurement accuracy of attitude angle and attitude angular velocity are 0.05 deg (3σ) and 0.0005 deg/s (3σ), respectively. And, the empirical model of attitude disturbance is given by

$$\boldsymbol{\delta} = \begin{cases} A_0(3\cos(\omega_o t) + 1) \\ A_0(1.5\sin(\omega_o t) + 3\cos(\omega_o t)) \\ A_0(3\sin(\omega_o t) + 1) \end{cases} \tag{79}$$

where $A_0 = 1.5 \times 10^{-5}$N·m, ω_o is orbit angular velocity of the servicing spacecraft.

The other simulation parameters are listed as table 1.

Table 1. Simulation Parameters.

Variable	Value	Unit
$\boldsymbol{I}_s$	diag([160, 190, 200])	kg·m^2
$\boldsymbol{I}_t$	diag([150, 180, 210])	kg·m^2
$\boldsymbol{\rho}_0$	$[50/\sqrt{2}, 0, 50/\sqrt{2}]^{\mathrm{T}}$	m
$\dot{\boldsymbol{\rho}}_0$	$[-0.15, 0.2, -0.1]^{\mathrm{T}}$	m/s
$\boldsymbol{q}_t$	$[0.5477, 0.6, -0.5, 0.3]^{\mathrm{T}}$	——
$\boldsymbol{q}_s$	$[0.9961, 0.04, -0.05, 0.06]^{\mathrm{T}}$	——
$\boldsymbol{\omega}_t$	$[-3, 2, 3]^{\mathrm{T}}$	deg/s
$\boldsymbol{\omega}_s$	$[-0.02, 0.01, 0.02]^{\mathrm{T}}$	deg/s
ω_o	0.001	rad/s
$[\Omega\ i\ \omega\ \theta_0]$	[30, 45, 10, 0]	deg
a	6920	km
e	0.005	——
a_{max}	1.5	m/s^2
T_{max}	4.5	N·m

Where a, e, i, Ω, ω, θ_0, are the target orbit's initial parameters, a_{max} is the maximum control acceleration, T_{max} is the maximum control torque.

Selecting $\boldsymbol{k} = \mathrm{diag}([0.3,0.3,0.3,0.2,0.2,0.2])$, b=0.875, k_0=0.001, $\boldsymbol{\lambda}$=diag([0.4,0.4,0.4,0.03,0.03,0.03]. The first approaching phase is set to start at 0 second, and the second approaching phase is set to start at 100 second, the simulation is conducted and the results are showing as follows.

Scenario 1: the inertia moment of the servicing spacecraft and target are exactly known.

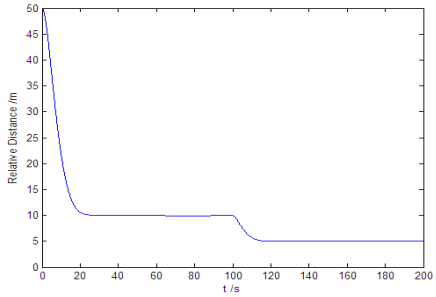

Figure 1. Relative distance between the centers of servicing spacecraft and target.

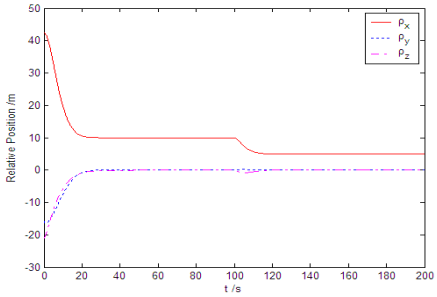

Figure 2. Relative position in the target body-fixed frame.

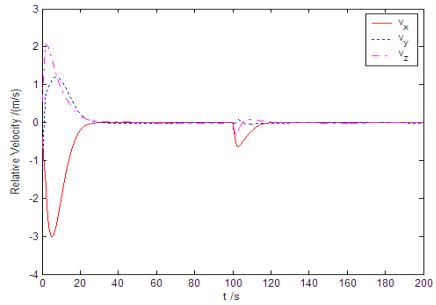

Figure 3. Relative velocity in the target body-fixed frame.

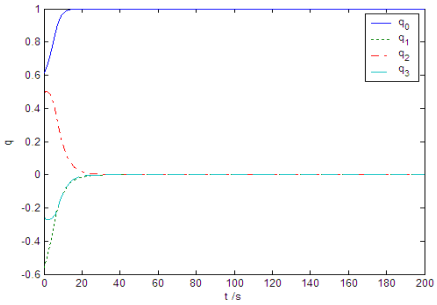

Figure 4. Relative Attitude Quaternion.

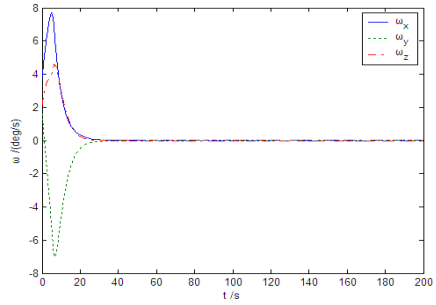

Figure 5. Relative Attitude Angular Velocity.

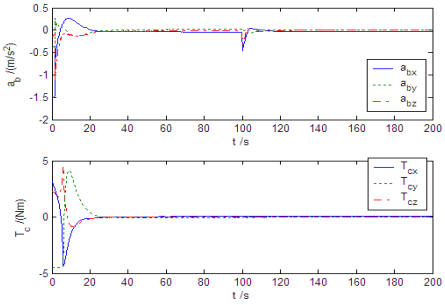

Figure 6. Control Accelerations and Control Torques.

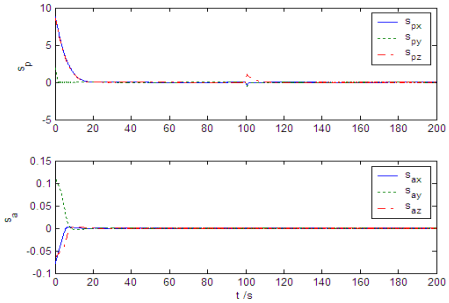

Figure 7. The First Sliding Surface.

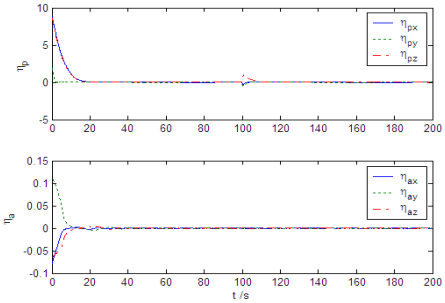

Figure 8. The Second Sliding Surface

Fig. 1 shows the relative distance of the servicing spacecraft from the target. Fig. 2 shows the relative position expressed in the target body-fixed frame. It shows that the transient response of relative position is very stationary and there's no oscillation during approaching. The initial relative distance is 50 meters, and the control objective is to drive the servicing spacecraft to a relative position of [5,0,0] meters in the target body-fixed frame and maintain it at this relative position. As can be seen, it takes about 30 seconds to reach the position of [10, 0, 0] meters in the target body-fixed frame. And it takes about 20 seconds to reach the position of [5, 0, 0] meters from the position of [10, 0, 0] meters expressed in the target body-fixed frame. The final relative position errors are ±[0.8, 3.4, 3.25] cm. The relative velocity's response curve in the target body-fixed frame is shown in Fig. 3, and the accuracy of the final relative velocity is better than ±1.02 cm/s. The relative attitude quaternion and the relative attitude angular velocity are shown in Figs. 4 and 5. The relative attitude quaternion converges to [1, 0, 0, 0] after 40 seconds. This indicates the servicing spacecraft's attitude is synchronized with the target's attitude, at this time, the docking port of servicing spacecraft has pointed to the docking port of the tumbling target. And the accuracy of the relative attitude angular velocity is better than $\pm 3\times 10^{-3}$deg/s. The results show a good position and attitude tracking performance. Fig. 6 shows the control accelerations and control torques. The first sliding surface and the second sliding surface in present of measurement noise are shown in Figs. 7 and 8, respectively. And, s_p, η_p are the sliding mode of relative position, s_a, η_a are the sliding mode of relative attitude. These results validate the effectiveness of the integrated coupled control law, in presence of external disturbances and measurement noise.

Scenario 2: the inertia moment of the servicing spacecraft and target are both perturbed by -50% uncertainties.

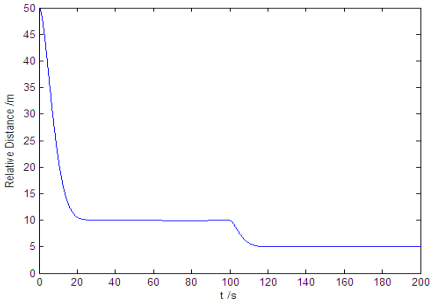

Figure 9. Relative distance between the centers of servicing spacecraft and target.

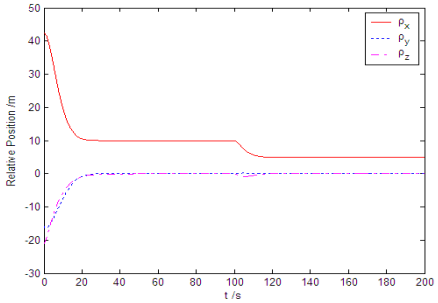

Figure 10. Relative position in the target body-fixed frame.

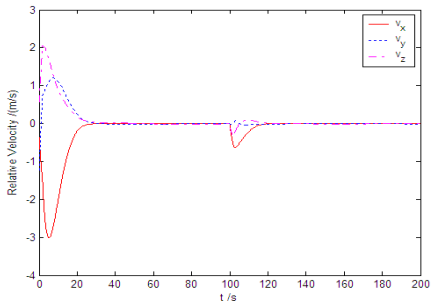

Figure 11. Relative velocity in the target body-fixed frame.

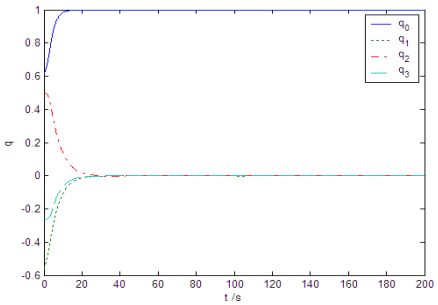

Figure 12. Relative attitude quaternion.

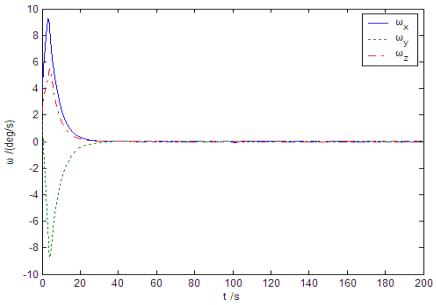

Figure 13. Relative attitude angular velocity.

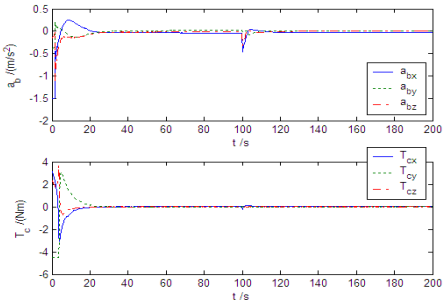

Figure 14. Control accelerations and control torques.

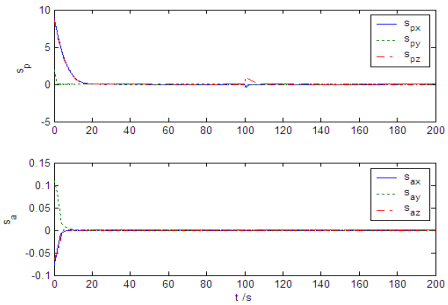

Figure 15. The first sliding surface.

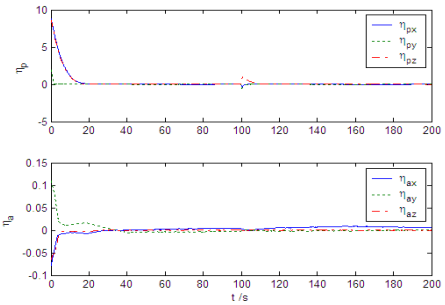

Figure 16. The second sliding surface.

The results show that it takes about 30 seconds to reach the position of [10, 0, 0] meters in the target body-fixed frame. And it takes about 20 seconds to reach the position of [5, 0, 0] meters from the position of [10, 0, 0] meters expressed in the target body-fixed frame. The final relative position errors are ±[0.8, 3.19, 3.25] cm. The accuracy of final relative velocity is better than ±1.00 cm/s. The relative attitude quaternion converges to [1, 0, 0, 0] after 45 seconds, the accuracy of the relative attitude angular velocity is better than $\pm 3 \times 10^{-3}$deg/s. Figs. 9-16 show that the relative position tracking and attitude synchronization are still so good that there isn't too much difference from Figs. 1-8.

Scenario 3: the inertia moment of the servicing spacecraft and target are both perturbed by 50% uncertainties, the relative perturbation accelerations and the disturbance torques are both enlarged 10 times (which can represent the uncertainties of the system).

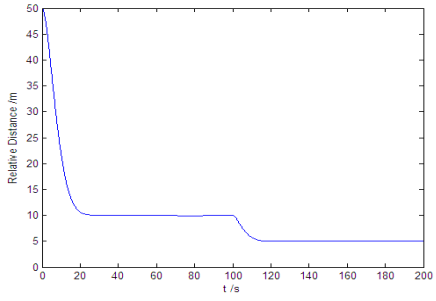

Figure 17. Relative distance between the centers of servicing spacecraft and target.

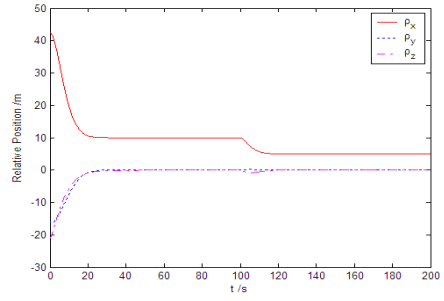

Figure 18. Relative position in the target body-fixed frame.

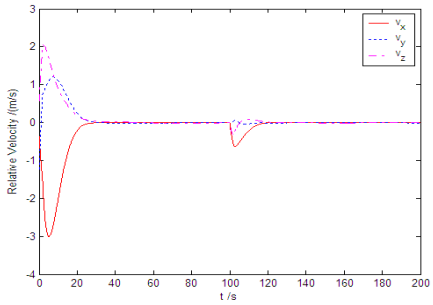

Figure 19. Relative velocity in the target body-fixed frame.

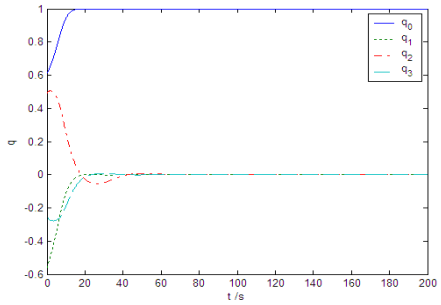

Figure 20. Relative attitude quaternion.

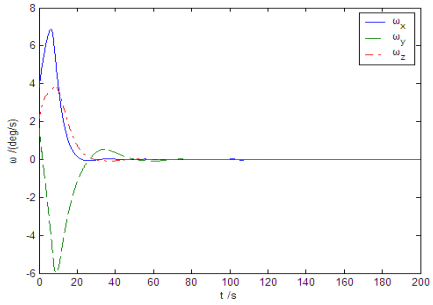

Figure 21. Relative attitude angular velocity.

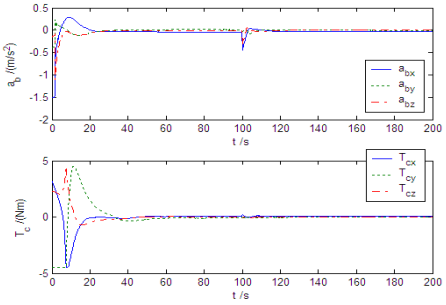

Figure 22. Control accelerations and control torques.

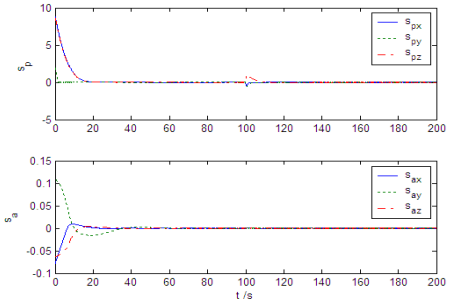

Figure 23. The first sliding surface.

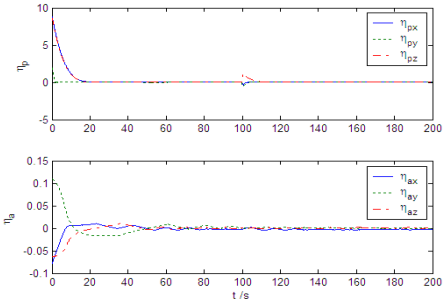

Figure 24. The second sliding surface.

The results show that it takes about 30 seconds to reach the position of [10, 0, 0] meters in the target body-fixed frame. And it takes about 20 seconds to reach the position of [5, 0, 0] meters from the position of [10, 0, 0] meters expressed in the target body-fixed frame. The final relative position errors are ±[0.8, 3.02, 3.15] cm. The accuracy of the final relative velocity is better than ±1.02 cm/s. The relative attitude quaternion converges to [1, 0, 0, 0] after 55 seconds, the accuracy of the relative attitude angular velocity is better than $\pm 5 \times 10^{-3}$deg/s. Figs. 17-24 show that the relative position tracking and attitude synchronization are still so good that there isn't too much difference from Figs. 1-8. All the previous simulation results show that the integrated coupled control law performs well and shows great robustness to parameter uncertainties and model uncertainties.

6. Conclusion

The coupled control problem of a servicing spacecraft autonomously approaching and docking with a tumbling target was studied. An integrated coupled control strategy was proposed to solve this problem. Docking with a tumbling target was accomplished through the scheme of relative position tracking and attitude synchronization, which achieved the docking port of the servicing spacecraft pointed to the docking port of the target during the final approaching and docking. The integrated coupled dynamics of relative position and attitude was established through relative position vector and relative attitude quaternion. And, based on this integrated coupled dynamics, a robust sliding mode control technique was developed to design the integrated coupled control law. The robustness of the integrated coupled control law to unknown but bounded disturbances, model uncertainties and measurement noise were all analyzed. Finally, three numerical simulation scenarios were conducted, and the results verified the effectiveness and robustness of the proposed control law.

Acknowledgment

Research for this paper was supported by the China Postdoctoral Science Foundation (20090450126) and the State High-Tech Development Plan (2010AA7020101).

References

[1] S. Croomes, "Overview of the DART Mishap Investigation Results", NASA Report, **(2006)**.

[2] T. M. Davis and D. Melanson, "XSS-10 Micro-Satellite Flight Demonstration Program", Proceedings of SPIE, vol. 5419, **(2004)**, pp. 16-25.

[3] L. David, "Military Micro-sat Explores Space Inspection, Servicing Technologies", http://www.space.com/businesstechnology/050722_XSS-11_test.html.

[4] M. A. Dornheim, "Orbital Express to Test Full Autonomy for On-orbit Service", http://www.aviationnow.com/avnow/news/channel_awst_story.jsp?id=news/aw060506p1.xml.

[5] R. B. Friend, "Orbital Express Program Summary and Mission Overview", Proceedings of SPIE, vol. 6958, **(2008)**, pp. 695803-1-695803-11.

[6] S. Nolet and D. W. Miller, "Autonomous Docking experiments using the SPHERES Testbed inside the ISS", Proceedings of SPIE, vol. 6555, **(2007)**, pp. 65550P-1-65550P-12.

[7] S. C. Lo and Y. P. Chen, "Smooth Sliding-Mode Control for Spacecraft Attitude Tracking Maneuvers", Journal of Guidance, Control, and Dynamics, vol. 18, **(1995)**, pp. 1345-1349.

[8] S. Laghrouche, F. Plestan and A. Glumineau, "Higher Order Sliding Mode Control Based on Integral Sliding Mode", Automatica, vol. 43, **(2007)**, pp. 531-537.

[9] J. M. Daly and D. W. L. Wang, "Output Feedback Sliding Mode Control in the Presence of Unknown Disturbances", Systems & Control Letters, vol. 58, **(2009)**, pp. 188-193.

[10] W. Luo, Y. C. Chu and K. V. Ling, "H_∞ Inverse Optimal Attitude-Tracking Control of Rigid Spacecraft", Journal of Guidance, Control, and Dynamics, vol. 28, **(2005)**, pp. 481-493.

[11] Z. X. Li and B. L. Wang, "Robust Attitude Tracking Control of Spacecraft in the Presence of Disturbances", Journal of Guidance, Control, and Dynamics, vol. 30, pp. 1156-1159.

[12] G. Harnischmacher and W. Marquardt, "Nonlinear Model Predictive Control of Multivariable Processes Using Block-Structured Models", Control Engineering Practice, vol. 15, **(2007)**, pp. 1238-1256.

[13] S. K. Scarritt, "Nonlinear Model Reference Adaptive Control for Satellite Attitude Tracking", AIAA Guidance, Navigation and Control Conference and Exhibit, AIAA 2008-7165.

[14] I. Ali, G. Radice and J. Kim, "Backstepping Control Design with Actuator Torque Bound for Spacecraft Attitude Maneuver", Journal of Guidance, Control, and Dynamics, vol. 33, **(2010)**, pp. 254-259.

[15] F. Terui, "Position and Attitude Control of a Spacecraft by Sliding Mode Control", Proceedings of the American Control Conference, **(1998)**, pp. 217-221.

[16] D. T. Stansbery and J. R. Cloutier, "Position and Attitude Control of a Spacecraft Using the State-Dependent Riccati Equation Technique", Proceedings of the American Control Conference, **(2000)**, pp. 1867-1871.

[17] P. Singla, K. Subbarao and J. L. Junkins, "Adaptive Output Feedback Control for Spacecraft Rendezvous and Docking Under Measurement Uncertainty", Journal of Guidance, Control, and Dynamics, vol. 29, **(2006)**, pp. 892-902.

[18] K. Subbarao and S. Welsh, "Nonlinear Control of Motion Synchronization for Satellite Proximity Operations", Journal of Guidance, Control, and Dynamics, vol. 31, **(2008)**, pp. 1284-1294.

[19] M. Xin and H. Pan, "Integrated Nonlinear Optimal Control of Spacecraft in Proximity Operations", International Journal of Control, vol. 83, **(2010)**, pp. 347-363.

[20] M. D. J. Brown, "Continuous and Smooth Sliding Mode Control", Ph.D. dissertation, University of Alabama in Huntsville, Dept. of Electrical and Computer Engineering, chap. 8, **(2001)**, pp, 117-120.

[21] B. Wie and J. Lu, "Feedback Control Logic for Spacecraft Eigenaxis Rotations Under Slew Rate and Control Constraints", Journal of Guidance, Control, and Dynamics, vol. 18, **(1995)**, pp. 1372-1379.

[22] M. D. Lichter and S. Dubowsky, "State, Shape, and Parameter Estimation of Space Objects from Range Images", Proceedings of the 2004 IEEE International Conference on Robotics & Automation, **(2004)**, pp. 2974-2979.

[23] U. Hillenbrand and R. Lampariello, "Motion and Parameter Estimation of a Free-Floating Space Object from Range Data for Motion Prediction", 8th International Symposium on Artificial Intelligence, Robotics and Automation in Space, **(2005)**.

[24] S. G. Kim, J. L. Crassidis, Y. Cheng and A.M. Fosbury, "Kalman Filtering for Relative Spacecraft Attitude and Position Estimation", Journal of Guidance, Control, and Dynamics, vol. 30, **(2007)**, pp. 133-143.

[25] F. Aghili and K. Parsa, "Adaptive Motion Estimation of a Tumbling Satellite Using Laser-Version Data with Unknown Noise Characteristics", Proceedings of the 2007 IEEE/RSJ International Conference on Intelligent Robots and Systems, **(2007)**, pp. 839-846.

[26] F. Aghili and K. Parsa, "An Adaptive Vision System for Guidance of a Robotic Manipulator to Capture a Tumbling Satellite with Unknown Dynamics", Proceedings of the 2008 IEEE/RSJ International Conference on Intelligent Robots and Systems, **(2008)**, pp. 839-846.

[27] Y. B. Shtessel and J. M. Buffington, "Continuous Sliding Mode Control", Proceedings of the American Control Conference, **(1998)**, pp. 562-563.

[28] M. D. J. Brown, Y. B. Shtessel and J. M. Buffington, "Finite Reaching Time Continuous Sliding Mode Control with Enhanced Robustness", Proceedings of AIAA Guidance, Navigation, and Control Conference and Exhibit, AIAA-2000-3964.

[29] G. Bartolini and P. Pydynowski, "An Improved Chattering Free, V.S.C. Scheme for Uncertain Dynamical Systems", IEEE Transactions on Automatic Control, vol. 41, **(1996)**, pp. 1220-1226.

[30] G. Bartolini, A. Ferrara and E. Usai, "Chattering Avoidance by Second-Order Sliding Mode Control", IEEE Transactions on Automatic Control, vol. 41, **(1998)**, pp. 241-246.

Authors

LU Wei received B. E. & M. E. degrees in Spacecraft Design from the Harbin Institute of Technology, China, in 2006 and 2008 respectively. Currently, he is a Ph. D. Candidate in Spacecraft Design from the Harbin Institute of Technology, Harbin, China. He has published about 2 refereed journal and conference papers. His research interest covers Sliding Mode Control, Robust Control, and Autonomous docking with a tumbling target. E-mail: luwei.spacecraft@gmail.com (Corresponding Author).

GENG Yunhai received B. E. degree in Engineering Mechanics from the Tongji University, M. E. degree and Ph. D degree in Spacecraft Design from the Harbin Institute of Technology, China, in 1992, 1995 and 2003 respectively. Currently, he is a Professor and doctoral advisor of Spacecraft Design, Harbin Institute of Technology, China. He has published about 60 refereed journal and conference papers. His research interest covers Spacecraft Attitude and Orbit Control , and Spacecraft Dynamics Navigation Guidance and Control (GNC) technology. E-mail: gengyh@hit.edu.cn.

CHEN Xueqin received B. E. degree in Automation, M. E. degree in Spacecraft Design and Ph. D degree in Control Science & Engineering from the Harbin Institute of Technology, China, in 2003, 2005 and 2008 respectively. Currently, she is a lecture of Spacecraft Design, Harbin Institute of Technology, China. She has published about 20 refereed journal and conference papers. Her research interest covers fault diagnosis and fault-tolerant control. E-mail: cxqhit@hit.edu.cn.

ZHANG Fan received B. E. degree in Automation and M. E. degree in Spacecraft Design from the Harbin Institute of Technology, China, in 2008 and 2010 respectively. Currently, he is a Ph. D. Candidate in Control Science & Engineering from the Harbin Institute of Technology, Harbin, China. He has published about 3 refereed journal and conference papers. His research interest covers Coordinated Control, Spacecraft Formation Flying. E-mail: autoctrllab@gmail.com.